ASEC 2022

MDPI

Proceeding Paper

First Principles Study on the Features of $Ca_xSr_{2-x}Ta_2O_7$ (x = 0, 1) as Photocatalytic Materials †

Marianela Gómez-Toledo *, Khalid Boulahya and M. Elena Arroyo-de Dompablo

Departamento de Química Inorgánica, Universidad Complutense de Madrid, 28040 Madrid, Spain; khalid@ucm.es (K.B.); mearroyo@ucm.es (M.E.A.-d.D.)

* Correspondence: mgom09@ucm.es

† Presented at the 3rd International Electronic Conference on Applied Sciences; Available online: https://asec2022.sciforum.net/.

Abstract: With hydrogen becoming one of the energetic vectors widely used in the future, the decarbonization of the energy sector requires an increase in hydrogen production from renewable resources. Materials that are able to catalyze the water-splitting reaction through sunlight absorption have been widely studied as an adequate solution for green hydrogen generation. Among the proposed tantalum-based oxide materials, $Sr_2Ta_2O_7$ displays photocatalytic activity. Aiming to improve the photocatalytic properties by means of compositional modifications, this work presents a DFT study of the Sr substitution by Ca. The structural, energetic, and electronic features of $Ca_xSr_{2-x}Ta_2O_7$ ($0 < x < 1$) phases have been examined. The computational results utilizing the SCAN functional show that there is a slight decrement in the band gap value (from 3.65 eV for x = 0 to 3.50 eV for x = 1) concomitant to a minor distortion of the crystal structure.

Keywords: $Sr_2Ta_2O_7$; green hydrogen; photocatalysis; water splitting; DFT

Citation: Gómez-Toledo, M.; Boulahya, K.; Dompablo, E.A.-d. First Principles Study on the Features of $Ca_xSr_{2-x}Ta_2O_7$ (x = 0, 1) as Photocatalytic Materials. **2022**, *4*, x. https://doi.org/10.3390/xxxxx

Academic Editor(s):

Published: 1 December 2022

1. Introduction

Climate change might be one of the biggest challenges that we face nowadays as a society. Currently, most of the produced energy come from fossil fuels, which contributes to greenhouse gas emissions. Energy production through renewable sources is being explored as a solution to this major issue. In that respect, hydrogen (H_2) seems to be the energetic vector of the future [1,2]; it presents a high combustion efficiency and the highest energy content per unit mass of all fossil fuels normally used [3]. However, hydrogen production rarely comes from zero-emission sources. In this sense, hydrogen production through water splitting using sunlight (i.e., photocatalysis) presents a key to green hydrogen generation [4] (p. 3).

Photocatalytic dissociation of water can be achieved using semiconductor materials that are able to absorb sunlight, leading to the promotion of electrons from the valence band (VB) to the conduction band (CB). There are, however, some vital concerns that must be considered: the VB maximum should be below the O_2/H_2O oxidation potential (1.23 eV) and the CB minimum should be above the H_2O/H_2 reduction potential (0.0 eV). Likewise, the band gap should be smaller than 3.0 eV to use visible light and larger than 1.23 eV to fulfill band position requirements [5]. Several compounds have been studied for this purpose, for example, TiO_2, WO_3, CdSe, CdS, or Ta_2O_5 [6]. Among the investigated oxides, $Sr_2Ta_2O_7$ [7,8] shows some exciting characteristics, particularly its CB position relative to

H_2O/H_2 reduction potential. However, its large band gap (4.6 eV) limits the light absorption to the UV region of sunlight.

The $Sr_2Ta_2O_7$ compound presents a perovskite-derived structure [9], where four perovskite layers form 2D nets perpendicular to the *c* axis, as shown in Figure 1. In the ABO_3 perovskite blocks, Ta occupies the B position, being coordinated to 6 O atoms. Sr can be in two different positions, Sr(1) and Sr(2), that are coordinated to 8 and 12 O atoms, respectively. Sr(1) can be described as an atom between perovskite blocks layers, while Sr(2) can be seen as an atom inside those blocks.

Previous computational studies [10,11] suggest that anion and cation doping in the Ta site can lead to an enhancement of the band gap value and the relative positions of the bands. As for cation doping in the Sr site, some authors [12] have experimentally demonstrated that the partial substitution of Sr for Ba can improve photocatalytic activity. Specifically, the solid solution $Sr_{2-x}Ba_xTa_2O_7$ was successfully synthetized in the compositional range $0 < x < 0.4$, with the term $x = 0.4$ displaying the best catalytic performance. This makes appealing the investigation of the substitution of Sr with other cations such as Ca, that could potentially enhance the photocatalytic activity of $Sr_2Ta_2O_7$. For this purpose, this work focuses on the computational study through DFT calculations of the structural and electronic changes that the substitution of Sr with Ca can provoke in the $Ca_xSr_{2-x}Ta_2O_7$ family. In particular, the $x = 0$ and 1 phases are studied.

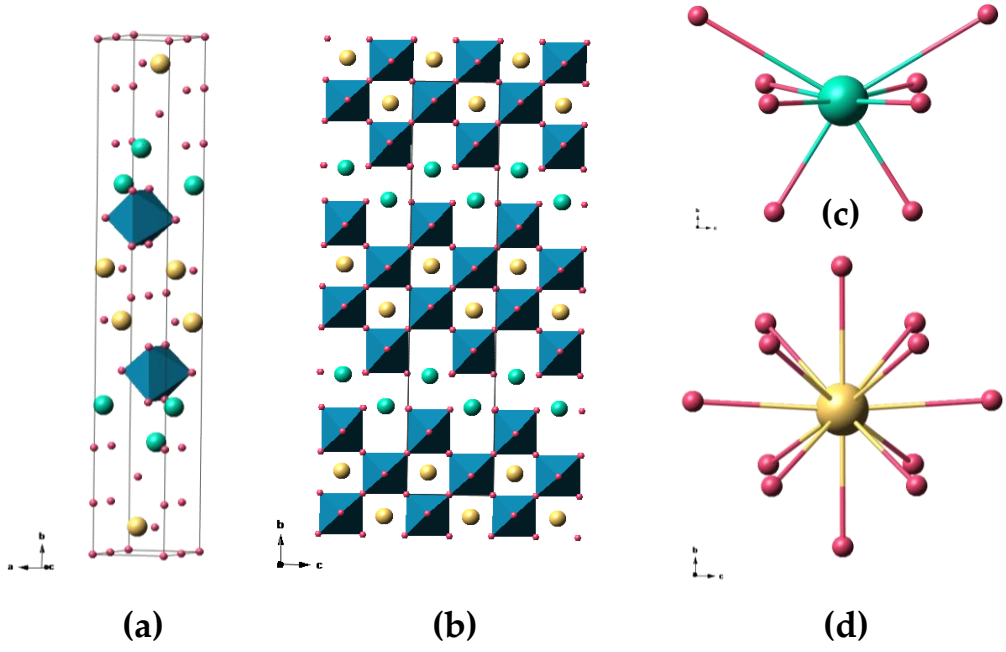

Figure 1. (**a**) Unit cell of $Sr_2Ta_2O_7$ [S.G. *Cmcm* (No.63)]; (**b**) Layered structure perpendicular to the *c* axis in $Sr_2Ta_2O_7$; (**c**) Detail of the Sr(1) coordination environment; (**d**) Detail of Sr(2) coordination environment. Ta atoms are shown in blue, O in red, Sr(1) in green and Sr(2) in yellow.

2. Materials and Methods

2.1. Crystallographic Models

Crystallographic models were built from $Sr_2Ta_2O_7$ structure (ICSD file 601) [9]. The structure was used to model $Sr_{2-x}Ca_xTa_2O_7$ family, where $x = 1$. However, since there are two possibilities for the Sr substitution (Figure 1), two models with Ca were constructed. The substitution of Sr(1) for Ca led to the model named $CaSrTa_2O_7$(1), and the substitution of Sr(2) for Ca generated the model named $CaSrTa_2O_7$(2).

2.2. Computational Methods

DFT calculations have been performed using VASP package (Vienna ab-initio simulation package) developed at the Universität Wien [13,14]. The Projector Augmented Wave (PAW) [15] method was used to describe the interaction of core electrons with nuclei, specifically 4*s*4*p*5*s* for Sr, 5*p*6*s*5*d* for Ta, 2*s*2*p* for O, and 3*s*3*p*4*s* for Ca were treated as valence electrons. A meta-GGA exchange-correlation functional was utilized, in particular, the recently developed strongly constrained and appropriately normed (SCAN) [16]. The energy cutoff was set at 600 eV throughout all calculations. Integration of the first Brillouin zone was carried out under the determination of k-points by the Monkhorts-Pack scheme. The k-point meshes were set at 6 x 2 × 6 in all cases, along with a Gaussian smearing parameter of 0.05 eV. For the density of states (DOS) calculations, the tetrahedron method with Bloch corrections [17] was employed. The tolerance threshold in total energy to achieve self-consistency was set at 1E-4 eV. Structural relaxation was performed over atoms' position, as well as cell shape and volume. No symmetry constrains where imposed during relaxation for the Ca models calculations.

3. Results and Discussion

3.1. Crystal Structure

Structural optimization results for $Sr_2Ta_2O_7$ within the SCAN functional are shown in Table 1. Lattice parameters obtained are in good agreement with experimental measurements [9], with errors below 0.5%. Likewise, distances results are, in general, in line with experimental values, showing deviations below 4.5%. Thus, the SCAN functional can correctly reproduce the crystal structure of $Sr_2Ta_2O_7$.

Table 1. Lattice parameters and atomic distances in $Sr_2Ta_2O_7$ (S.G. *Cmcm*) structure and $CaSrTa_2O_7$ models (S.G. *Cmcm*).

Lattice parameters (Å)					
	$Sr_2Ta_2O_7$			**$CaSrTa_2O_7$(1)**	**$CaSrTa_2O_7$ (2)**
	Experimental	**Calculated**	**% Error**	**Calculated**	**Calculated**
a	3.9376	3.9537	0.4	3.9084	3.9273
b	27.1986	27.1894	0.03	27.0999	27.0855
c	5.6927	5.6951	0.04	5.6119	5.6646
Volume (Å^3)	609.50	612.22	0.4	594.40	602.56
Distances (Å)					
	$Sr_2Ta_2O_7$			**$CaSrTa_2O_7$(1)**	**$CaSrTa_2O_7$ (2)**
	Experimental	**Calculated**	**% Error**	**Calculated**	**Calculated**
Sr1/Ca1-O	2.47 (x4)	2.480	0.4	2.416	2.469
Sr1/Ca1-O	2.60 (x2)	2.575	1.0	2.435	2.572
Sr1/Ca1-O	3.27 (x2)	3.313	1.3	3.338	3.347
Sr2/Ca2-O	2.71 (x4)	2.719	0.3	2.697	2.653
Sr2/Ca2-O	2.827 (x4)	2.837	0.4	2.809	2.848
Sr2/Ca2-O	2.85 (x2)	2.852	0.1	2.811	2.849
Sr2/Ca2-O	2.70	2.629	2.6	2.650	2.476
Sr2/Ca2-O	2.74	2.743	0.1	2.731	2.721
Ta1-O	1.87 (x2)	1.855	0.8	1.871	1.859
Ta1-O	1.979 (x2)	1.989	0.5	1.976	1.990
Ta1-O	2.16 (x2)	2.071	4.1	2.141	2.128
Ta2-O	1.89 (x2)	1.855	1.9	1.832	1.907
Ta2-O	1.98 (x2)	1.997	0.9	1.969	1.978
Ta2-O	2.07 (x2)	2.157	4.2	2.067	2.032

Regarding the relative stability of the two crystallographic models proposed for $CaSrTa_2O_7$, DFT calculations show that the $CaSrTa_2O_7$(1) model has lower energy than $CaSrTa_2O_7$(2) model (energy difference of 332 meV). The relative stability can be rationalized considering the ionic radii of Ca^{2+} (r = 1.12 Å for C.N. = 8 and 1.34 Å for C.N. = 12 [18]) and Sr^{2+} (r = 1.26 Å for C.N. = 8 and 1.44 Å for C.N. = 12 [18]). This calculated energy indicate that a more stable structure is formed if the larger Sr^{2+} occupies the position inside perovskite blocks (C.N. = 12), which is to say, the smaller Ca^{2+} cation will tend to occupy the site between perovskite layers position (C.N. = 8).

Lattice parameters and atomic distances for the most stable $CaSrTa_2O_7$ model are listed in Table 1. As expected, the introduction of the smaller Ca^{2+} ion produces a contraction of the unit cell, and a reduction of all lattice parameters. Overall, the introduction of Ca ions preserves the initial structure of $Sr_2Ta_2O_7$.

3.2. Electronic Structure

Figures 2 and 3 show the calculated density of states and band structure of the $Sr_2Ta_2O_7$ and DOS of $CaSrTa_2O_7$ models, respectively.

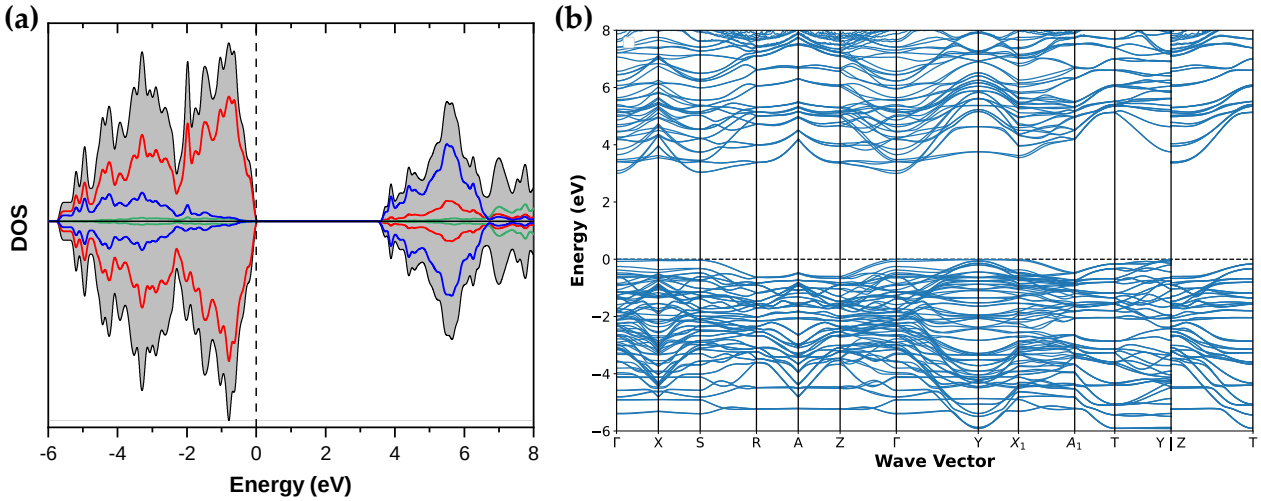

Figure 2. (**a**) Calculated density of states of $Sr_2Ta_2O_7$. (**b**) Calculated band structure of $Sr_2Ta_2O_7$. The Fermi level is set at the zero of energy. Color code: total black, O red, Sr green, Ta blue.

The DOS for $Sr_2Ta_2O_7$ is represented in Figure 2a. The Fermi level is set at 0 of energy. The VB is mainly formed by 2*p* states of O while CB is composed of 5*d* Ta states. Hybridization exists between O and Ta states in both bands. Sr barely contributes to forming the valence and conduction bands, thus is not expected that substitution of the mentioned cation led to a big change in electronic structure. Despite this, in d^0 transition metals oxides perovskites, the substitution can provoke a distortion in crystal structure which could ultimately change electronic structure [19]. As shown in Figures 2a and b, a direct band gap of 3.65 eV is obtained using SCAN functional. This result deviates from the experimental one (4.6 eV), given that band gap underestimation is a known failure of DFT methods [20].

Despite the limitations of DFT to reproduce accurate band-gap values, the trends in band-gaps due to chemical composition modifications are fully reliable [11].

Figure 3 shows DOS for the two models used to simulate the $CaSrTa_2O_7$ compounds. $CaSrTa_2O_7$(1) has a band gap of 3.55 eV while $CaSrTa_2O_7$(2) band gap is 3.50 eV. Therefore, calculations suggest that in the $Sr_{2-x}Ca_xTa_2O_7$ family the trend is to reduce the band gap as x increases. Importantly, band gap variations are of only about 0.15 eV when going from x = 0 to x = 1. Additionally, valence and conduction bands in $CaSrTa_2O_7$ models have essentially the same features as in the $Sr_2Ta_2O_7$ phase.

Considering the exposed results, the substitution of Sr with Ca in $Sr_2Ta_2O_7$, only leads to a slight reduction of the band gap value, independently of the Ca position. This seems insufficient to cause an effective change in the photocatalytic activity of the material. Taking into account the experimentally observed improvement of photocatalytic activity when substituting Sr with Ba in some $Sr_{2-x}Ba_xTa_2O_7$ phases [12], more work is needed to (1) asses the effects of the Sr substitution in $Sr_2Ca_2O_7$ with Ca/Ba and other cations and (2) study additional features that could account for an improved catalytic activity, such as the electron-hole recombination.

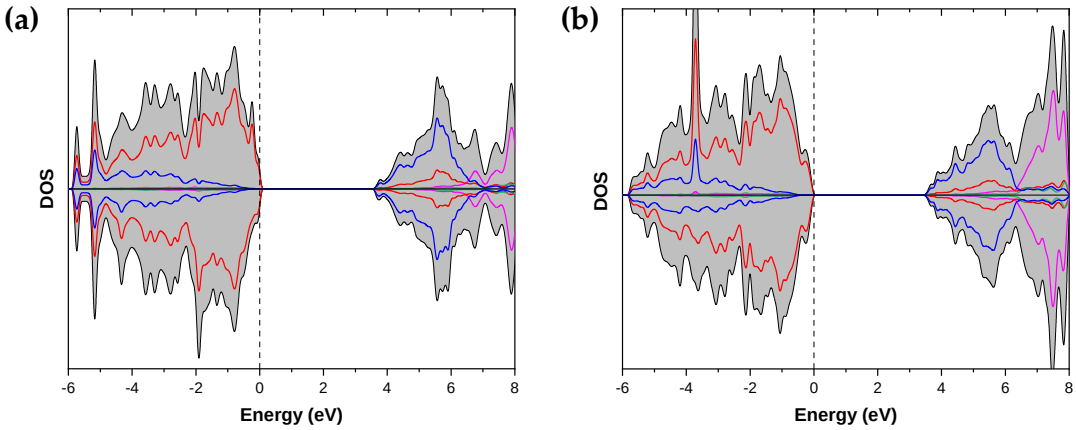

Figure 3. Calculated density of states of (**a**) $CaSrTa_2O_7$(1) and (**b**) $CaSrTa_2O_7$(2). The Fermi level is set at the zero of energy. Color code: total black, O red, Sr green, Ca pink, Ta blue.

4. Conclusions

Computational investigations at the level of Density Functional Theory (DFT) permit predicting some basic and critical features in view of the photocatalytic activity of materials. In this work DFT methods are used to predict the crystal and electronic structures of the potential photocatalyst $Sr_{2-x}Ca_xTa_2O_7$. We found that the x = 1 phases preserve the perovskite-related structure of the parent $Sr_2Ta_2O_7$. The calculated DOS shows a band narrowing of 0.10–0.15 eV because of Sr substitution with Ca. With band gaps of ~4.5 eV sunlight absorption by the $SrCaTa_2O_7$ photocatalyst is limited to the UV region. Work is in progress to investigate other substitutions that may enhance the photocatalytic activity of $Sr_2Ta_2O_7$.

Author Contributions: M.G.-T.: methodology, formal analysis, investigation, data curation, writing-original draft preparation, visualization. K.B.: conceptualization, validation, resources. M.E.A.-d.D.: conceptualization, supervision, project administration, funding acquisition. All authors have read and agreed to the published version of the manuscript.

Funding: Universidad Complutense de Madrid (FEI-EU-22-01- 4129585) and Comunidad de Madrid (PEJ-2020-AI/IND-18065).

Institutional Review Board Statement:

Informed Consent Statement:

Data Availability Statement:

Acknowledgments: Authors thanks I. Collado and R. Carrasco for contributions in the experimental data analysis.

Conflicts of Interest: The authors declare no conflict of interest.

References

1. Abdin, Z.; Zafaranloo, A.; Rafiee, A.; Mérida, W.; Lipiński, W.; Khalilpour, K.R. Hydrogen as an energy vector. *Renew. Sustain. Energy Rev.* **2020**, *120*, 109620. https://doi.org/10.1016/j.rser.2019.109620.
2. Dawood, F.; Anda, M.; Shafiullah, G.M. Hydrogen production for energy: An overview. *Int. J. Hydrogen Energy* **2020**, *45*, 3847–3869. https://doi.org/10.1016/j.ijhydene.2019.12.059.
3. Ishaq, H.; Dincer, I.; Crawford, C. A review on hydrogen production and utilization: Challenges and opportunities. *Int. J. Hydrogen Energy* **2022**, *47*, 26238–26264. https://doi.org/10.1016/j.ijhydene.2021.11.149.
4. Acar, C.; Dincer, I. Hydrogen Production. *Compr. Energy Syst.* **2018**, *3–5*, 1–40. https://doi.org/10.1016/B978-0-12-809597-3.00304-7.
5. Wang, Z.; Li, C.; Domen, K. Recent developments in heterogeneous photocatalysts for solar-driven overall water splitting. *Chem. Soc. Rev.* **2019**, *48*, 2109–2125. https://doi.org/10.1039/c8cs00542g.
6. Osterloh, F.E. Inorganic materials as catalysts for photochemical splitting of water. *Chem. Mater.* **2008**, *20*, 35–54. https://doi.org/10.1021/cm7024203.
7. Kato, H.; Kudo, A. New tantalate photocatalysts for water decomposition into H_2 and O_2. *Chem. Phys. Lett.* **1998**, *295*, 487–492.
8. Kudo, A.; Kato, H.; Nakagawa, S. Water Splitting into H2 and O2 on New Sr2M2O7 (M = Nb and Ta) Photocatalysts with Layered Perovskite Structures: Factors Affecting the Photocatalytic Activity. *J. Phys. Chem. B* **2000**, *104*, 571–575. https://doi.org/10.1021/jp9919056.
9. Ishizawa, N.M.F.; Kawamura, T.; Kimura, M. Compounds with Perovskite-Type Slabs. II. The Crystal Structure of Sr2Ta207. *Acta Crystallogr. Sect. B* **1976**, *B32*, 2564–2566.
10. Liu, P.; Nisar, J.; Ahuja, R.; Pathak, B. Layered perovskite Sr2Ta2O7 for visible light photocatalysis: A first principles study. *J. Phys. Chem. C* **2013**, *117*, 5043–5050. https://doi.org/10.1021/jp310945e.
11. Peng, Y.; Ma, Z.; Hu, J.; Wu, K. A first-principles study of anionic (S) and cationic (V/Nb) doped Sr2Ta2O7 for visible light photocatalysis. *RSC Adv.* **2017**, *7*, 40922–40928. https://doi.org/10.1039/c7ra07113b.
12. Kim, K.Y.; Eun, T.H.; Lee, S.-S.; Chon, U. Photocatalytic Activities and Structural Changes of Barium-Doped Strontium Tantalate. *Resour. Process.* **2009**, *56*, 138–144. https://doi.org/10.4144/rpsj.56.138.
13. Furthmüller, G.K.J. Efficient iterative schemes for ab initio total-energy calculations using a plane-wave basis set. *Phys. Rev. B* **1996**, *54*, 11169. https://doi.org/10.1103/PhysRevB.54.11169.
14. Kresse, G.; Joubert, D. From ultrasoft pseudopotentials to the projector augmented-wave method. *Phys. Rev. B* **1999**, *59*, 1758. https://doi.org/10.1103/PhysRevB.59.1758.
15. Bloch, P.E. Projector augmented-wave method. *Phys. Rev. B* **1994**, *50*, 17953. https://doi.org/10.1103/PhysRevB.50.17953.
16. Sun, J.; Ruzsinszky, A.; Perdew, J.P. Strongly Constrained and Appropriately Normed Semilocal Density Functional. *Phys. Rev. Lett.* **2015**, *115*, 036402. https://doi.org/10.1103/PhysRevLett.115.036402.
17. Blochl, P.E.; Jepsen, O.; Andersen, O.K. Improved Tetrahedron Method for Brillouin-Zone integrations. *Phys. Rev. B* **1994**, *49*, 16223–16233. https://doi.org/10.1103/PhysRevB.49.16223.
18. Shannon, R.D. Revised effective ionic radii and systematic studies of interatomie distances in halides and chaleogenides. *Acta Crystallogr. A* **1976**, *32*, 751. https://doi.org/10.1107/S0567739476001551.
19. Eng, H.W.; Barnes, P.W.; Auer, B.M.; Woodward, P.M. Investigations of the electronic structure of d0 transition metal oxides belonging to the perovskite family. *J. Solid State Chem.* **2003**, *175*, 94–109. https://doi.org/10.1016/S0022-4596(03)00289-5.
20. Borlido, P.; Schmidt, J.; Huran, A.W.; Tran, F.; Marques, M.A.L.; Botti, S. Exchange-correlation functionals for band gaps of solids: Benchmark, reparametrization and machine learning. *NPJ Comput. Mater.* **2020**, *6*, 96. https://doi.org/10.1038/s41524-020-00360-0.